

Elastic wave finite difference modelling as a practical exploration tool

Peter M. Manning and Gary F. Margrave

ABSTRACT

Finite difference modelling of elastic wavefields is now practical for elucidating features of records obtained for exploration seismic purposes. This has become possible because of the major increase in computing power available at reasonable cost. To take advantage of this power a 2D finite difference modelling program for elastic displacements has been written in Matlab. The program has then been used to investigate the propagation of surface waves through shallow layers with lateral and vertical changes. Some distinctive effects have been seen under ideal conditions, and it is hoped that these will also appear in realistic cases and provide practical interpretation methods.

INTRODUCTION

The continuing increase in computer power at affordable cost provides an ever-increasing target for its utilization. Modelling by finite difference methods requires powerful computer resources which has limited its applications in the past, but the present availability of computer power and user friendly languages means more finite difference applications are within reach. Modelling of surface waves is one possibility for finite difference methods, especially since ray-tracing methods can't be used.

Surface waves are an inevitable feature on seismic records and have usually been considered noise. However recent studies have found the shallow penetration of surface waves to be ideal for near surface investigations, especially for environmental purposes (Park et al, 1996). Techniques have been developed to interpret shallow bed thickness and near surface velocities from these surface waves (especially using velocity dispersion) (Xia et al, 1997).

It also appears that the large static shifts found on shear wave traces are caused by very shallow conditions. An understanding and interpretation of surface wave anomalies may then lead to improved shear wave statics. It may also be significant that surface wave velocities are quite closely related to shear wave velocities.

Surface waves in a uniform medium combine horizontal and vertical particle motion in a precisely defined relationship. The horizontal motion in the real earth may be important for interpreting conditions there, an aspect that has not received much coverage as yet. On the other hand, if the vertical and horizontal relationships

are usually predictable, this may be used to reduce the 'noise' caused by surface waves (possibly with a sophisticated form of polarization filter).

FINITE DIFFERENCE MODELLING

Elastic wave equations

The vector formulation of the elastic wave equation is

$$(\lambda + 2\mu)\nabla(\nabla \cdot \bar{u}) - \mu\nabla \times (\nabla \times \bar{u}) = \rho \frac{\partial^2 \bar{u}}{\partial t^2}. \quad (1)$$

where λ and μ are Lamé parameters, u is displacement, and ρ is density. Equation (1) may be formulated in 2D Cartesian coordinates as

$$(\lambda + 2\mu)\frac{\partial^2 u_x}{\partial x^2} + (\lambda + \mu)\frac{\partial^2 u_z}{\partial x \partial z} + \mu \frac{\partial^2 u_x}{\partial z^2} = \rho \frac{\partial^2 u_x}{\partial t^2}. \quad (2)$$

and a similar equation for the u_z acceleration with an exchange of x and z .

Finite difference representation

The principle feature of the physical representation chosen is the staggered grid as designed by Virieux in 1986. In this method the displacement values in the z direction refer to positions which are half way (in both x and z) between the positions for the displacement values in the x direction.

The spatial difference operators chosen were second order. The advantages relative to higher order methods are an obvious relationship to the physical parameters and faster run times per time step. The disadvantage is that a finer space and time sampling may be required for a given frequency range. It is hoped that increasing computer capacity will be sufficient to compensate for the lower efficiency and or accuracy of the second order approximation.

In contrast to the Virieux paper, the method chosen keeps track only of displacements and not tensions. Memory use is reduced by this means, at a cost of greater complexity, especially for boundary conditions.

Figure 1 shows the relevant positions of the parameters required to calculate the x displacement for the next time step. At the center of the diagram is the point where the x displacement will be calculated. Also marked are all the points which will influence the displacement at the next time step, 4 in the z direction and 4 in the x direction, as well as the point at the center itself. The points where the relevant shear

and compressional strengths apply are marked with symbols. Also shown are the relationships chosen for the indices to describe the parameters. To distinguish which grid an index refers to, m and n are used for the u_x grid, while j and k are used for the u_z grid.

Z displacement relationships are the same with components rotated 90 degrees except for some indexing adjustments.

The details of the finite difference representation on a staggered grid and its relationship to the continuous equation are given in the appendix.

Matlab coding

Matlab code for the 2D Cartesian case has been written and tested using simple sources with known theoretical results. When coded using a matrix to specify each parameter for the entire model, it has been found to be reasonably efficient, with a 500 metre offset, 1 second shot record running within 10 minutes (the space step was 2.5 metres and time step 0.5 milliseconds). There has not been any appreciable numerical dispersion with 30 Hz Ricker wavelets using the parameters to obtain these run times. Broader band wavelets will require more computer time but should still be practical. It will be important to limit numerical dispersion so that the physical velocity dispersion can be distinguished.

The code assumes that the model is symmetric about $x = 0$, the z -axis on the left edge. Symmetric models may then be initiated symmetrically about $x = 0$ and only half the calculation is needed. Models may be positioned away from the z axis at $+x$ but will act as if another model at $-x$ is also progressing.

Matlab debugging and plotting features have been found very useful. Especially useful has been the 'quiver' plot, which uses arrows to show the direction and amplitude of particle motion. An example of quiver is shown in figure 2.

Modelling examples

Figure 2 uses the 'quiver' plot to show a snapshot of displacements at 300 milliseconds after a shot is fired at (0,10) metres of a uniform half space (marked +). This example makes use of the modelling software assumption of symmetry about the axis at $x = 0$ to compute for only half of the volume. The events can be distinguished and are marked: with P for the pressure wave primary and ghost, with S for the shear wave ghost, with PS for the shear head wave converted from P at the surface, and with R for the surface (Rayleigh) wave.

Figure 3 is a conventional plot of Z component displacement at the surface after an explosion at (0,10) metres. The model has one low velocity layer 14m thick at the surface and an interface to much higher velocities at 125 m. The reflected wave, trapped waves, and surface waves are marked. The reflection can be seen mainly at long offsets (past 250m) even though the velocity and density contrasts are 2:1. The overwhelming amplitudes of the surface waves are partly due to the oversimplified shallow model.

FINITE DIFFERENCE MODELLING - CYLINDRICAL COORDINATES

To obtain amplitude relationships which are valid in three dimensions but only require two dimensional modelling, it is proposed to formulate the wave equation in cylindrical coordinates with the Z axis vertical at the source point. The results will be valid only in axially symmetric situations, but that includes many realistic cases.

The cylindrical formulation can be derived from equation (1) and are as follows:

$$(\lambda + 2\mu) \left(\frac{\partial^2 u_r}{\partial r^2} + \frac{1}{r} \frac{\partial u_r}{\partial r} - \frac{u_r}{r^2} \right) + (\lambda + \mu) \frac{\partial^2 u_z}{\partial r \partial z} + \mu \frac{\partial^2 u_r}{\partial z^2} = \rho \frac{\partial^2 u_r}{\partial t^2}. \quad (3)$$

$$(\lambda + 2\mu) \frac{\partial^2 u_z}{\partial z^2} + (\lambda + \mu) \left(\frac{\partial^2 u_r}{\partial r \partial z} + \frac{1}{r} \frac{\partial u_r}{\partial z} \right) + \mu \left(\frac{1}{r} \frac{\partial u_z}{\partial r} + \frac{\partial^2 u_z}{\partial r^2} \right) = \rho \frac{\partial^2 u_z}{\partial t^2}. \quad (4)$$

This method may provide more realistic amplitude relationships between body and surface waves.

STUDY OF SHALLOW LAYERS WITH SURFACE WAVES

Source wavelet

A specialized source wavelet was designed for study of surface waves, and a snapshot of it is shown in figure 4. The reasons for a special wavelet are: the limited depth penetration of a surface wave allows a relatively thin model and so requires lower running times, the low level of body wave energy ensures that the effects seen are mainly from surface waves, and the short surface wave package enables the effects to be more closely related to their causes and again lowers run times.

The surface wavelet is constructed from an arbitrary input wavelet, in this case a zero phase Ricker wavelet. The input wavelet is assumed to be the z component of the surface wavelet and the x component is derived by multiplying the derivative of the z component by the amplitude factors consistent with equations for theoretical surface wave displacements as discussed in Krebes (1989) p 4.3. The z and x components are then modified with depth using the same formulae and by assuming a dominant frequency. The result is only an approximate surface wave but works well in practice.

It propagates almost unchanged and does not create body waves with significant amplitudes.

The wavelet shown in figure 4 was designed to move toward the right, and has retrograde particle motion at the surface if moving right as surface waves are known to have (as in Krebs p 4.4). Figure 5 shows the wavelet after 40 ms and it can be seen to have largely preserved its shape. It can also be seen that the propagated wave is a little closer to the expected form, with relatively lower frequency content at greater depths (consistent with the equations in Krebs).

Modelling examples

The examples all begin with a 30 Hz Ricker surface wavelet in a perfect half space and show vertical displacements at the surface as time advances. The half space velocity for P waves is 2857 m/sec, and for shear waves is 1000 m/sec, and the density is 2 g/cc. The shallow layers have the same density and most have their S velocities multiplied by either 0.7 or 1.4. The exception is the test for comparison of relative P and S effects, where the P wave velocity is multiplied by 0.7.

Figure 6 shows the wavelet propagating on a uniform half space. This is the base case and can be seen to have almost no change in wavelet character with time. The velocity of propagation is slightly less than the shear wave velocity - consistent with theory (Krebs p 4.2).

In figure 7 the propagation is into a material with lower velocity and great thickness. A line marks the boundary. A small reflected surface wave propagates left and the transmitted surface wave propagates more slowly to the right undispersed.

The propagation into a material with higher velocity and great thickness is shown in figure 8. The reflected wave appears again with polarity opposite to figure 7 and the transmitted wave travels faster, as expected. The reflected wave at the right edge is an edge effect.

The dispersive effects of layering on surface waves is shown in figure 9 where the wavelet propagates into a high velocity layer 10 metres thick (the position marked by a box). The reflected wave and first part of the transmitted wave are very similar to the great thickness case (figure 8) but then the high-speed portion of the wavelet receives interference from the low velocity half space below.

The wavelet in figure 10 is propagating into a low velocity layer 10 metres thick. The dispersive effects are again obvious. The results at first are very similar to the low velocity great thickness case of figure 7, but eventually the higher velocity material below causes stronger effects. Some low amplitude events can be seen with a slope corresponding to the high velocity material.

Figure 11 shows the results caused by a low velocity 10 metre layer of limited extent (marked by a box). The dispersion can be seen to end at the end of the box.

Figure 12 shows the corresponding results from propagating the wavelet through a high velocity box of limited extent.

The dispersion caused by a low velocity layer of only 5 metres is shown in figure 13 and can be compared to figure 10 of 10 metres. The stronger dispersion effect is probably due to the more even partition of energy within the layer as compared to below the layer for this wavelet. The wavelet is the 30 Hz Ricker shown in figure 4.

The minor influence of a material's P wave velocity on the surface wave velocity is shown in figure 14. Here the P wave velocity in the 10 metre layer has been reduced to 70% of the half space velocity while the S wave velocity remained unchanged. It is very difficult to see the difference here from the uniform half space of figure 6.

Figure 15 shows the same data as figure 10 but with the traces from 50 metres offset and further shifted by the time equivalent to the half space shear wave velocity used here of 1000 metres/second. The surface wave velocity in the half space shows as a little slower than this velocity. Plots of real data with this type of shifting may have some value in finding near surface velocity changes.

CONCLUSIONS

Finite difference modelling in Matlab can provide very useful insights, especially for surface waves.

It is hoped that some of the surface wave indicators shown here can be detected in cases with more realistic character, and eventually with real data. The indicators may be summarized as follows:

Reflected waves - appearing at the point of velocity change. These may be apparent only where the change is abrupt.

Slope change - to the near surface velocity. Persistence at the surface velocity is dependent on the thickness of the new velocity material as well as its extent.

Amplitude change - associated with velocity changes but also with layer thickness and extent.

Velocity dispersion - the differing velocity associated with events of differing frequency. This is the classical indicator used by seismologists.

It should be noted that the terms shallow, surface, and abrupt are all as compared with a given wavelet frequency, so that different frequency wavelets can be used to detect layers of differing thickness for example.

APPENDIX

Physical layout of the staggered grid

The staggered grid provides a natural relationship between the x and z displacements so that their mutual interactions can be easily related as the model is stepped in time. Figure 1 is used for calculating u_x and shows all the displacements that will contribute for the next time step. To the lower left are the grid and the grid indices for all the u_x (displacements) that will contribute to the u_x at m,n for the next time step. There are also four u_z (displacements) on the upper right grid that will contribute to the new u_x .

The vector displacement at a given point can be obtained from the x or z displacement there plus the average of the four displacements surrounding that point for the other component. The x and z displacements can be mostly independent, just as crossing wavefields can be, but they do interact through the second term of the differential equation.

The differential wave equation for u_x acceleration can be used to calculate u_x at a later time. The equation is:

$$(\lambda + 2\mu) \frac{\partial^2 u_x}{\partial x^2} + (\lambda + \mu) \frac{\partial^2 u_z}{\partial x \partial z} + \mu \frac{\partial^2 u_x}{\partial z^2} = \rho \frac{\partial^2 u_x}{\partial t^2} \quad (1)$$

The finite difference representation chosen has a direct relation to the components of this equation. The relationships are explained below for each term on the left as it contributes to the acceleration on the right. The first and third terms are explained first because they are completely in u_x . The second term (in two parts) is then explained, and the advantage of the staggered grid for specifying the u_x/u_z interaction can be seen.

First term

The first term of the equation represents the force caused by the change in x displacement (u_x) with x . The finite difference terms can be built up from the physics with the following steps:

The horizontal force between $u_x(m+1,n)$ and $u_x(m,n)$ is compressional and given by

$$F_x(m+.5,n) = Lp2m(j,n)(u_x(m+1,n)-u_x(m,n))dydz/dx \quad (2)$$

In this equation $Lp2m = \lambda + 2\mu$, the unilateral compression factor, and its position is marked by the gray squares. The x co-ordinate of this factor (j) is on the u_z grid, and the z co-ordinate (n) is on the u_x grid. The m 's and n for F_x and u_x are on the u_x grid. $dydz$ represents the area where the displacements apply.

Similarly the horizontal force between $u_x(m,n)$ and $u_x(m-1,n)$ is given by

$$F_x(m-.5,n) = Lp2m(j-1,n)(u_x(m,n)-u_x(m-1,n))dydz/dx . \quad (3)$$

The net force is given by the difference between equations 2 and 3 and applies at $x = m$ to a box of size $dx dy dz$ and density ρ . The resultant acceleration in the x direction is

$$a_x(m,n) = (F_x(m+.5,n)-F_x(m-.5,n))/(dx dy dz \rho) . \quad (4)$$

Upon substitution of equations (2) and (3) in (4), the $dy dz$'s cancel and the dx 's square in the denominator, and this is the equation used in the finite difference code. It preserves the dependence of the compressional factor on x and z , and provides a natural way to include distinct geological formations within the model.

To show the relationship to the continuous case assume that the spacing is so fine that $Lp2m$ can be assumed constant and the resulting equation is

$$a_x(m,n) = Lp2m(j,n)(-u_x(m-1,n)+2u_x(m,n)-u_x(m+1,n))/((dx)^2 \rho) . \quad (5)$$

The three u_x terms represent the second derivative of u_x with x so that the continuous equivalent becomes

$$(\lambda + 2\mu) \frac{\partial^2 u_x}{\partial x^2} \frac{1}{\rho} = \frac{\partial^2 u_x}{\partial t^2} \quad (6)$$

which is the first term of the continuous equation.

Third term

The third term of the equation represents the force caused by the change in u_x with z . The finite difference terms are derived with the following steps:

The horizontal force between $u_x(m,n+1)$ and $u_x(m,n)$ is shear and given by

$$F_x(m,n+.5) = \mu u_x(m,k+1)(u_x(m,n+1)-u_x(m,n))dx dy / dz . \quad (7)$$

In this equation μ is the shear modulus, and its position is marked by the gray diamonds. The x co-ordinate of this factor (m) is on the u_x grid, and the z co-ordinate (k) is on the u_z grid. The m and n 's for F_x and u_x are on the u_x grid. $dx dy$ represents the area where the displacements apply.

Similarly the horizontal force between $u_x(m,n)$ and $u_x(m,n-1)$ is given by

$$F_x(m,n-.5) = \text{Mu}(m,k)(u_x(m,n)-u_x(m,n-1))dx dy/dz . \quad (8)$$

The net force is given by the difference between equations 7 and 8, and applies at $z = n$ to a box of size $dx dy dz$ and density ρ . The resultant acceleration in the x direction is

$$a_x(m,n) = (F_x(m,n+.5)-F_x(m,n-.5))/(dx dy dz \rho) . \quad (9)$$

Upon substitution of equations (7) and (8), the $dx dy$'s cancel and the dz 's square in the denominator, and the finite difference equation results.

To proceed to the continuous equation, assume Mu is constant and the result is

$$a_x(m,n) = \text{Mu}(m,k)*(-u_x(m,n-1)+2u_x(m,n)-u_x(m,n+1))/((dz)^2 \rho) . \quad (10)$$

The three u_x terms represent the second derivative of u_x with z so that the continuous equivalent becomes

$$\mu \frac{\partial^2 u_x}{\partial z^2} \frac{1}{\rho} = \frac{\partial^2 u_x}{\partial t^2} \quad (11)$$

which is the third term of the continuous equation.

Second term part λ

The second term of the equation is where the interaction between the displacements in x and z occur and where energy is transferred between the grids. The first part of the interaction describes the force in the x direction caused by the change in u_z with z . The finite difference terms are derived with the following steps:

The horizontal force caused by the difference between $u_z(j,k+1)$ and $u_z(j,k)$ is the unilateral compression case and given by

$$F_x(m+.5,n) = \text{Lambda}(j,n)(u_z(j,k+1)-u_z(j,k))dy dz/dz . \quad (12)$$

In this equation $\text{Lambda} = \lambda$, and its position is also marked by the same gray squares as the $Lp2m$ factor. The m and n for F_x is on the u_x grid and of course the u_z indices are on the u_z grid. $dy dz$ represents the area where the displacements apply.

Similarly the horizontal force caused by $u_z(j-1,k+1)$ and $u_z(j-1,k)$ is given by

$$F_x(m-.5,n) = \text{Lambda}(j-1,n)(u_z(j-1,k+1)-u_z(j-1,k))dydz/dz . \quad (13)$$

The net force is given by the difference between equations 12 and 13, and applies at $x = m$ to a box of size $dx dy dz$ and density ρ . The resultant acceleration in the x direction is

$$a_x(m,n) = (F_x(m+.5,n)-F_x(m-.5,n))/(dx dy dz \rho) . \quad (14)$$

Upon substitution of equations (12) and (13), the dy 's cancel and $dx dz$ is left in the denominator, and this is the finite difference equation. It can be seen that this equation uses the same u_z 's as (15) below, and they are equally weighted, so the fact that they surround the output point at m,n gives them the ideal position for influencing future displacements there. This is the reason for the staggered grid.

Where the spacing is so fine that Lambda can be considered constant the resulting equation is

$$a_x(m,n) = \text{Lambda}(j,n)((u_z(j,k+1)-u_z(j,k))/dz-(u_z(j-1,k+1)-u_z(j-1,k))/dz)/dx \rho . \quad (15)$$

Each pair of u_z terms represents the first derivative of u_z with z , and the combination of the pairs represents the first derivative of them with x so that the continuous equivalent becomes

$$\lambda \frac{\partial^2 u_z}{\partial x \partial z} \frac{1}{\rho} = \frac{\partial^2 u_x}{\partial t^2} \quad (16)$$

which is part of the second term of the continuous equation.

Second term part μ

The second part of the $u_x u_z$ interaction describes the force in the x direction caused by the change in u_z with x . The finite difference terms are derived with the following steps:

The horizontal force caused by the difference between $u_z(j,k+1)$ and $u_z(j-1,k+1)$ is shear and given by

$$F_x(m,n+.5) = \mu u(m,k+1)(u_z(j,k+1)-u_z(j-1,k+1))dydz/dz . \quad (17)$$

Similarly the horizontal force caused by $u_z(j,k)$ and $u_z(j-1,k)$ is given by

$$F_x(m,n-.5) = \mu u(m,k)(u_z(j,k)-u_z(j-1,k))dydz/dz . \quad (18)$$

The net force is given by the difference between equations 17 and 18, and gives an acceleration in the x direction of

$$a_x(m,n) = (F_x(m,n+.5)-F_x(m,n-.5))/(dx dy dz \rho) . \quad (19)$$

and by the same reasoning as above gives

$$\mu \frac{\partial^2 u_z}{\partial x \partial z} \frac{1}{\rho} = \frac{\partial^2 u_x}{\partial t^2} \quad (20)$$

which is the second part of the second term of the continuous equation. Again it is obvious that the four input u_z terms surround the output location, the ideal result allowed for by the staggered grid positioning.

References:

- Krebes, E. S., 1989, Geophysics 551 seismic theory and methods – course notes: unpublished.
- Park, C. B., Miller, R. D., Xia, J., 1996, Multi-channel analysis of surface waves using vibroseis: Expanded abstracts 1996 SEG International Exposition, 68-71.
- Virieux, J., 1986, P-SV wave propagation in heterogeneous media: Velocity – stress finite difference method: Geophysics, **51**, 889-901.
- Xia, J., Miller, R. D. and Park, C. B., 1997, Estimation of shear wave velocity in a compressible Gibson half-space by inverting Rayleigh wave phase velocity: Expanded abstracts 1997 SEG International Exposition, 1917-1920.

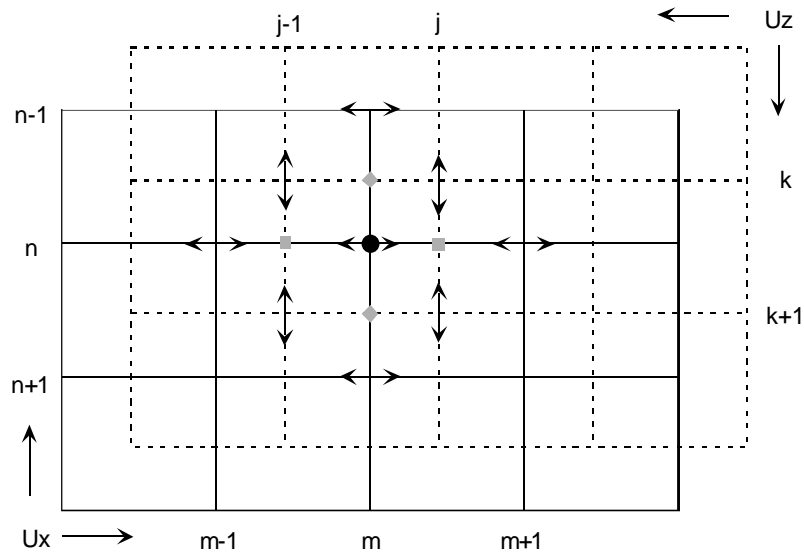


Fig 1: The staggered grid for displacement representation. Compressional parameters are required at the gray squares, shear parameters at the gray diamonds.

Vector displacement at 300 ms – source 10 m

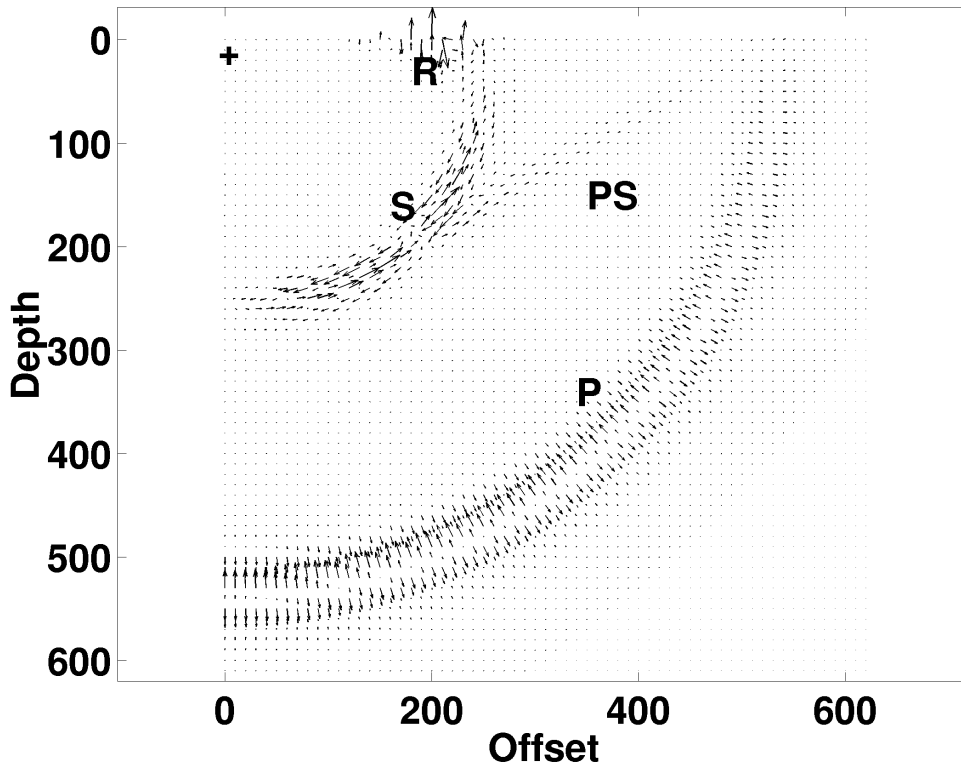


Fig 2: Cartesian 2D finite difference snapshot at 300 ms after an explosive source at (0,10) m (marked +). Events include the P wave primary plus ghost (P), shear wave ghost (S), shear head wave (PS), and surface (Rayleigh) wave (R).

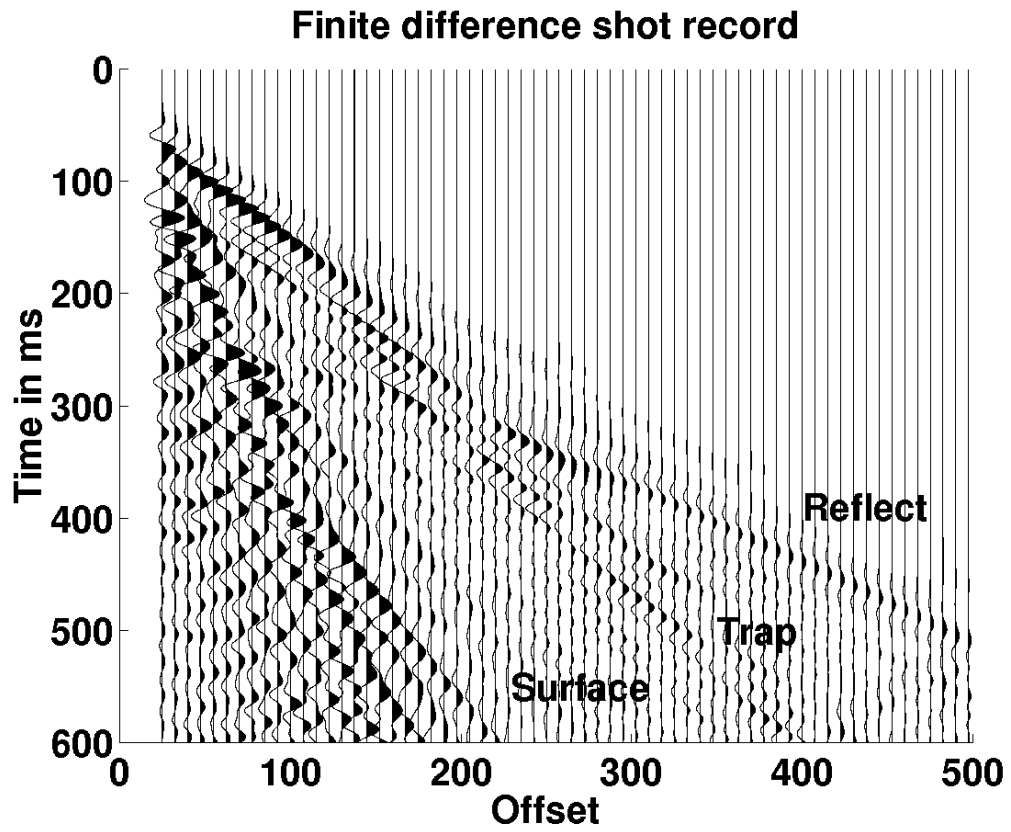


Fig 3: Finite difference seismogram from a buried explosive source showing trapped waves, surface waves, and one reflection.

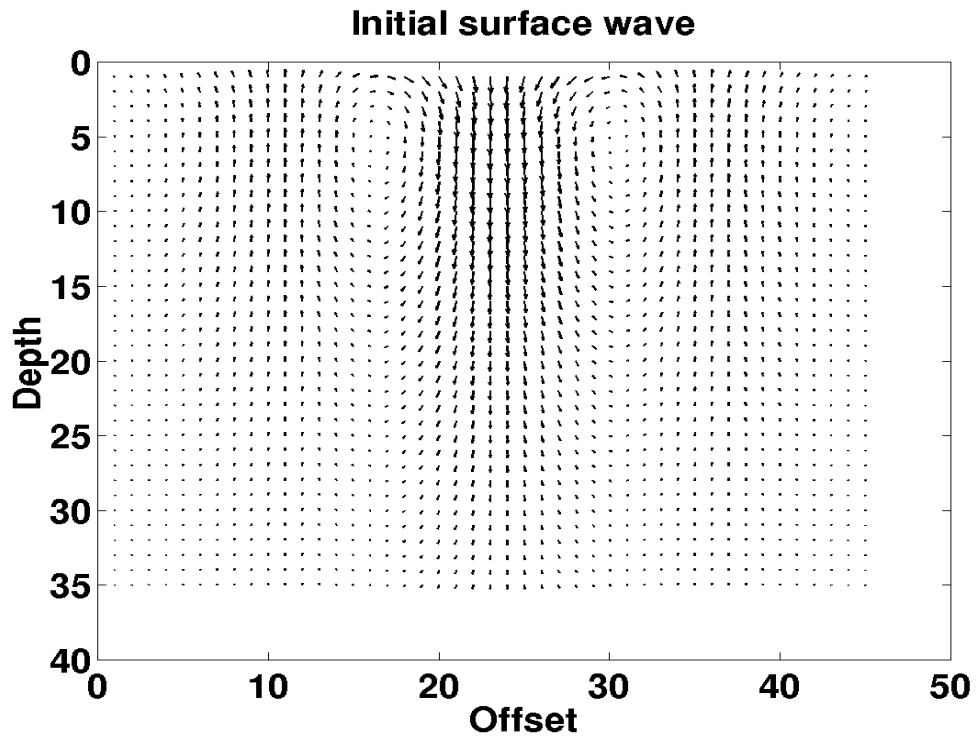


Fig 4: Snapshot of surface wave at time zero.

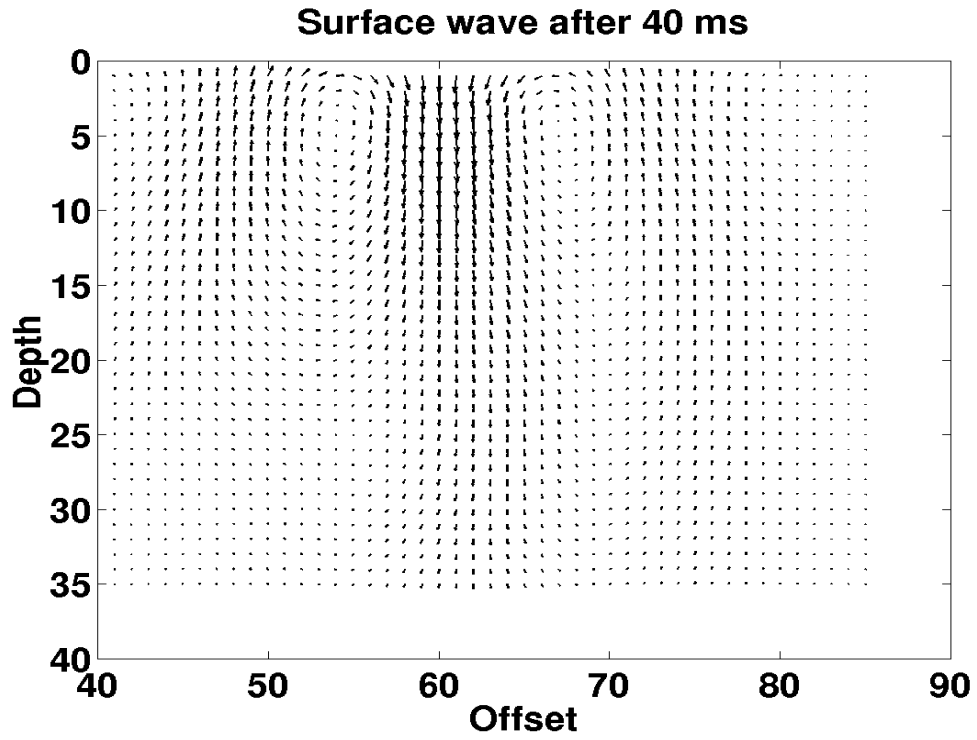
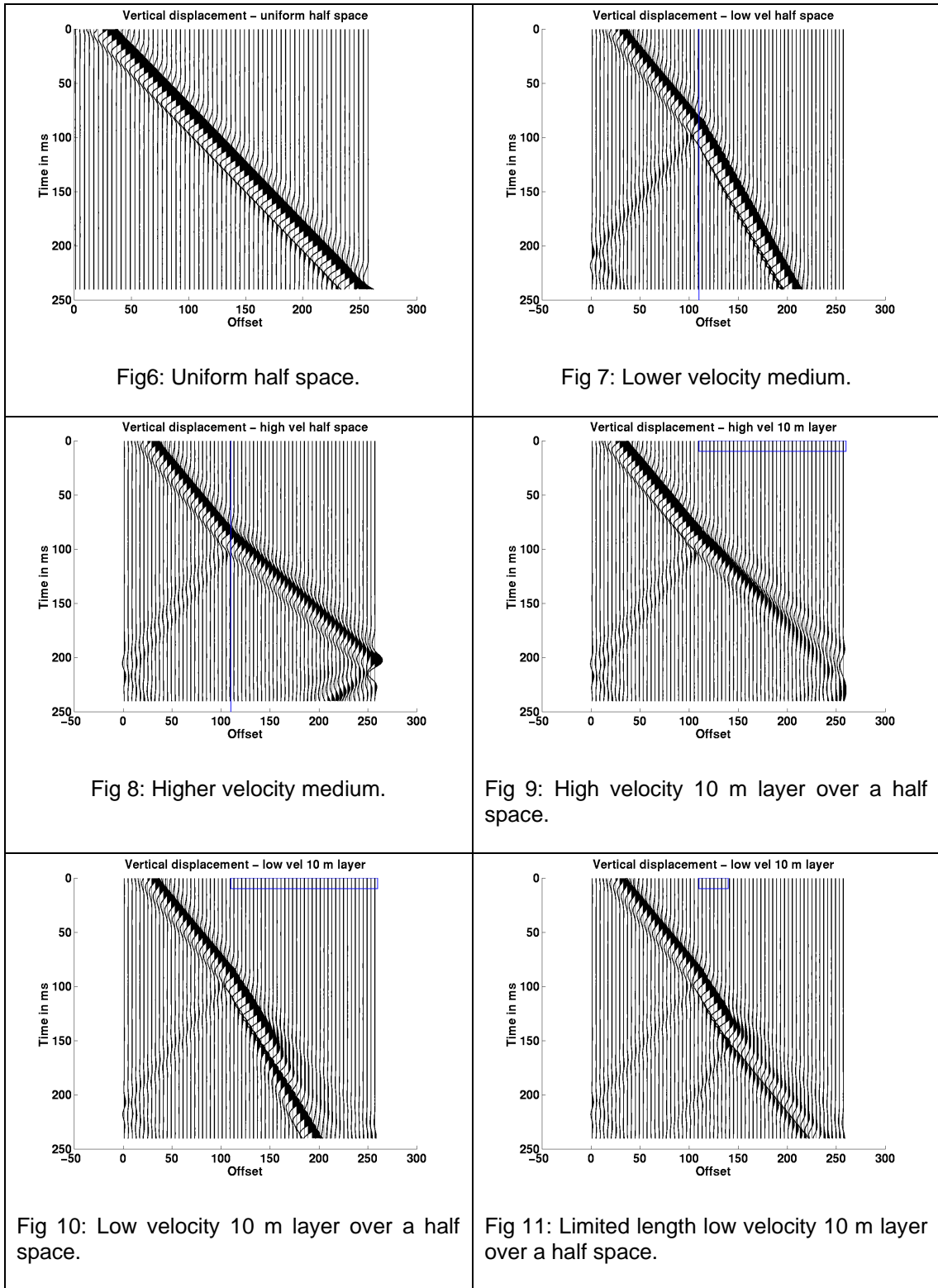


Fig 5: Snapshot of surface wave after propagation for 40 milliseconds.

Propagation of a surface wave into media of differing shear velocity structure.



Propagation of a surface wave into media of differing velocity structure.

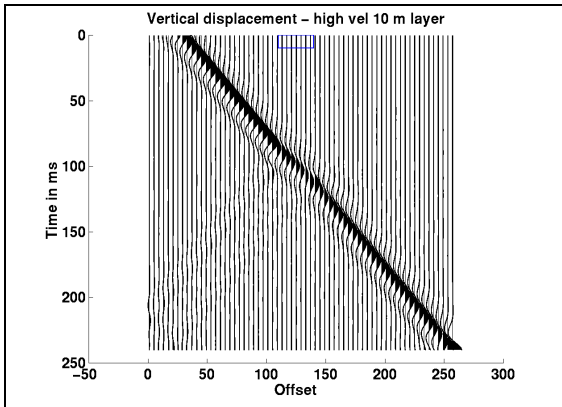


Fig 12: Limited length high velocity 10 m layer over a half space.

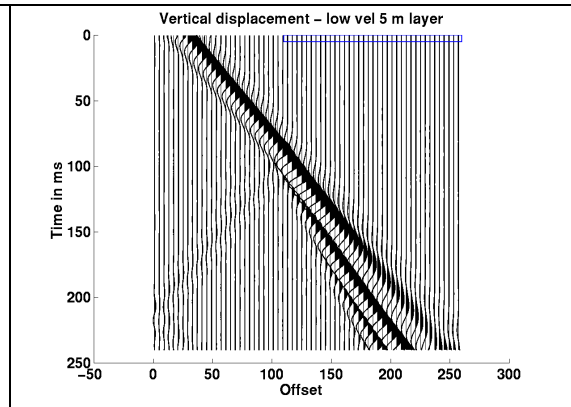


Fig 13: Low velocity 5 m layer over a half space.

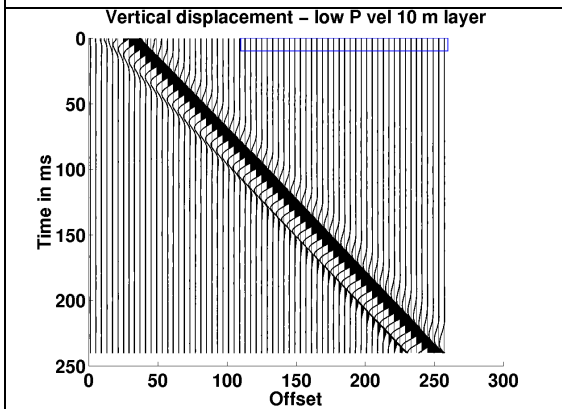


Fig 14: Low velocity P wave layer of 10 m over a half space.

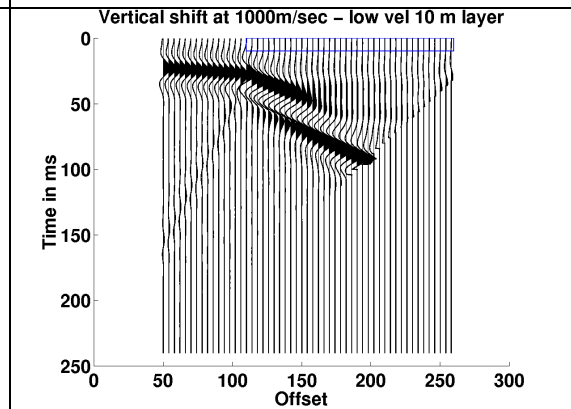


Fig 15: Time shifted traces of a 10 m low velocity layer over a half space.